Influence of ice formation on the dynamic and thermodynamic properties of aqueous solutions

Journal of Molecular Liquids 356 (2022) 119039

Contents lists available at ScienceDirect

Journal of Molecular Liquids

journal homepage: www.elsevier.com/locate/molliq

Influence of ice formation on the dynamic and thermodynamic properties of aqueous solutions

Jorge H. Melillo [a,c], Jan Swenson [b], Silvina Cerveny [a,c,*]

[a] Centro de Física de Materiales (CSIC-UPV/EHU)-Material Physics Centre (MPC), Paseo Manuel de Lardizabal 5 (20018), San Sebastián, Spain
[b] Department of Physics, Chalmers University of Technology, Göteborg, Sweden
[c] Donostia International Physics Center (DIPC), Paseo Manuel de Lardizabal 4 (20018), San Sebastián, Spain

ARTICLE INFO

Article history:
Received 17 December 2021
Revised 25 March 2022
Accepted 27 March 2022
Available online 30 March 2022

Keywords:
Water dynamics
Biological and conventional solutions
Crossover
Ice
Broadband
Dielectric spectroscopy

ABSTRACT

Water dynamics in solutions with biological or non-biological solutes has been intensely studied when both components (solvent and solute) are amorphous. Here, we apply broadband dielectric spectroscopy combined with calorimetric measurements to analyze the dynamics of the aqueous solutions tripropylene glycol (3PG) and ε-poly (lysine) (ε-PLL), after their water becomes semi-crystalline. Various crystallization levels were explored by conducting experiments with different annealing times at temperatures above the glass transition temperature (T_g). We find that the amount of ice depends on both the time and temperature of the annealing, and that this, in turn, affects T_g and dynamics of the amorphous part of the samples. However, it should be noted that the observed differences are relatively small for the degrees of crystallinity we have studied (up to about 26 wt% of the water). This also implies that the dynamic crossover of the water relaxation from a high temperature non-Arrhenius behavior to a low temperature Arrhenius dependence is unaffected by the partial crystallization and still occurs as a single crossover at the calorimetric T_g. Thus, we cannot detect two different crossovers, as commonly observed for other types of two-component systems, such as two glass formers.

1. Introduction

The study of water mixtures with diverse solutes (polymers [1,2], biopolymers [3–6], salts, amino acids [4,7] or other liquids [8]) is essential in technological applications and crucial to different phenomena connected with life (those involving proteins and other biomolecules in crowded solutions). Therefore, this field remains under intense investigation. Furthermore, in some cases, such as cryopreservation of stem cells, embryos for test-tube fertilization, and body organs before transplantations, icing of hydrated systems is harmful and should therefore be avoided if possible [9]. Nevertheless, it is crucial to understand how ice formation affects the water dynamics and distorts the hydrogen bonds between the solvent and the solute [10,11]. Moreover, water is not a passive solvent in many types of systems. Rather, it takes part in, e.g., metabolic enzymatic reactions and protein dynamics, which may be severely affected by partial crystallization of the surrounding water.

From a fundamental perspective, water shows several anomalies [12] that are more pronounced when water is supercooled [13] below its freezing/melting temperature of 0 °C. In particular, to explain these anomalies, a liquid–liquid transition (LLT) has been proposed using molecular dynamic simulations [14–16]. In an LLT, there is a change between a low-density liquid to a high-density liquid, and for bulk water, it has been proposed to occur below the homogeneous nucleation temperature (~235 K) [17]. The experimental evidence for an LLT in water has remained elusive because of the rapid crystallization of bulk water in the temperature range from 150 to 235 K.

The water dynamics in solutions with synthetic or biological materials has been deeply analyzed in the literature when the solution remains amorphous (i.e., solute and water are in the amorphous state). In this case, we know that "conventional" solutions only show two relaxations [1,2] (the viscosity-related structural α-relaxation and a faster relaxation of hydration/interfacial water). The temperature dependences of their relaxation times $\tau_\alpha(T)$ and $\tau_{water}(T)$ determined by dielectric spectroscopy [18], nuclear magnetic resonance [19], or quasi-elastic neutron scattering [20,21] have shown that $\tau_{water}(T)$ exhibits a crossover at the glass transition temperature (T_g) of the solution (see Fig. 1a, where the temperature dependence of the relaxation times are schematically shown). On the other hand, in the case of biological solutions and a reduced set of synthetic materials (such as poly(vinyl

* Corresponding author.
E-mail addresses: scerveny@ctq.csic.es, silvina.cerveny@ehu.es (S. Cerveny).

https://doi.org/10.1016/j.molliq.2022.119039
0167-7322/

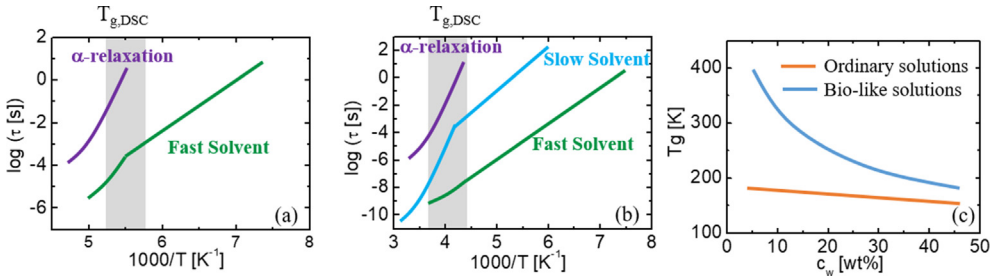

Fig. 1. Temperature dependence of the relaxation times for: (a) ordinary solutions with two relaxations (α- and water-relaxations) and (b) bio-like solutions with three relaxations (α-relaxation, slow- and fast-water relaxation). The grey area indicates the glass transition temperature. (c) Water concentration dependence of the glass transition temperature for both types of solutions.

pyrrolidone) (PVP)) [22,23], it is possible to identify an extra water related relaxation (as we call slow-water relaxation) in addition to the two relaxations mentioned above for "conventional" solutions. This additional water relaxation is faster than the structural α-relaxation, but slower than the other and universal water relaxation. Consequently, this category of solutions presents three relaxations (α-relaxation, slow- and fast-water relaxation, see Fig. 1b) for which both the slow- and fast- water relaxations show a single crossover at T_g. These dynamic crossovers, produced in the two types of solutions, are of interest for understanding the dynamical properties of supercooled water under soft confinements and making predictions of a scenario for supercooled bulk water [24]. The requirement for observing all three types of dynamics is that the variation of the glass transition temperature with water concentration is significant (more than 100 degrees) in the range from ~ 0 to 50 wt% water [22] (see Fig. 1c).

The dynamics of conventional solutions have also been studied under annealing to form some ice [25–28]. The main result is that annealing produces an increase of the glass transition temperature compared to the T_g of the amorphous state, since the unfreeze-concentrated phase decreases. It has been also reported that, by annealing water solutions, it is possible to observe the liquid–liquid transition in water [16,27]. However, later reports [25] showed that the T_g shift is due to a change in the water concentration when a part of the water crystallizes into ice. Bio-solutions were also studied in the presence of ice [19,29–31]. It has been observed that ice forms in solutions of collagen or elastin with hydration levels of 0.3 g/g, but the relaxation times of water remain unaffected [29]. Feldman and co-workers studied the dynamics of water and ice, both in bulk [32,33] and in aqueous solutions [34,35] of lysozyme. In this case, two crossovers were identified [35] for the water relaxation. The crossover at ~155 K corresponds to the calorimetry glass transition, while the crossover at ~186 K was assigned to the melting of water confined in the protein.

This work analyzes the dynamics of water in a semi-crystalline environment for the two categories of solutions (i.e., solutions that display two or three relaxations). We performed calorimetric and dynamical studies on water solutions of the glass-forming materials tri-propylene glycol (3PG) and ε-poly(lysine) (ε-PLL), with the aim to elucidate the influence of ice on the behavior of the water relaxation (for conventional solutions) and the fast-water relaxation (for aqueous solutions with multiple water relaxations). Specifically, we want to determine the number of dynamical crossovers observed in the water relaxation and whether the crossover temperatures are affected by ice in the solutions.

2. Experimental

2.1. Samples:

Tri-propylene glycol (3PG, M_W = 192.25 g/mol) was purchased from Sigma Aldrich, and (ε-poly(lysine) (ε-PLL, M_W = 4700 g/mol) was supplied by JNC Corporation (Japan). After lyophilization, the solutes were purified using an ion transfer resin (AG 501-X8, Bio-Rad Laboratories). Water (Sigma Aldrich water 95289) was added to the appropriate water concentration (c_w = 50 wt%) to prepare the aqueous solutions. In the case of ε-PLL, the samples were sealed for at least six months before being used. Such a long time was used because the water relaxation was found to change during up to 5 months of storage, probably because the water causes some slow conformational alterations of ε-PLL, which in turn affect how the water interacts with ε-PLL.

2.2. Calorimetric characterization:

Differential scanning calorimetry (DSC) measurements were performed using Q2000 TA equipment in the temperature-modulated mode (TMDSC). The total heat flow (HF) is equivalent to standard DSC, the reversing signal provides information on heat capacity and melting, whereas the non-reversing signal shows the kinetic events, such as the cold crystallization here studied. In TMDSC mode, a periodic temperature perturbation is superimposed to a linear heating or cooling. TMDSC experiments were carried out with different temperature amplitudes T_A = 0.08, 0.32 and 0.8 K using scanning rates of 0.5, 2 and 5 K/min, respectively. The modulation period was 60 s (ω = 0.105 rad s^{-1}). To compare the signals at different heating rates, normalization by the heating rate was done. Samples weighing about 10 to 15 mg were prepared in hermetic pans. Different temperature protocols were applied to measure the amorphous and the crystalline samples, as shown in Fig. 2.

2.3. Dynamical characterization:

The dynamics of the solutions were studied by broadband dielectric spectroscopy (BDS). The complex dielectric permittivity, ε*(ω) = ε'(ω) – i ε"(ω), was measured in the frequency domain using a Novocontrol Alpha-A$^+$ analyzer in the frequency range from 10^{-1} to 10^6 Hz and in the temperature range from 140 to 300 K. Samples were prepared forming a parallel-plate capacitor between gold-plated electrodes with a diameter of 20 mm and a thickness of 0.1 mm. The dielectric response was described by using the phenomenological Havriliak-Negami function for the α-relaxation and symmetric Cole-Cole functions for the water related relaxations.

$$\varepsilon^*(\omega) = \varepsilon_\infty + \sum_j \Delta\varepsilon(1 + (i \cdot \omega \cdot \tau_j)^{\alpha_j})^{-\beta_j} \quad (1)$$

where $\Delta\varepsilon = \varepsilon_s - \varepsilon_\infty$, with ε_∞ and ε_s being the un-relaxed and relaxed values of the dielectric constant, and τ_j is the characteristic relaxation time. α_j and β_j are the shape parameters ($0 \leq \alpha_j * \beta_j \leq 1$ and $0 \leq \alpha_j \leq 1$) which describe the symmetric and asymmetric broadening of the relaxation. The Cole-Cole function is the same as in eq. (1) with β = 1.

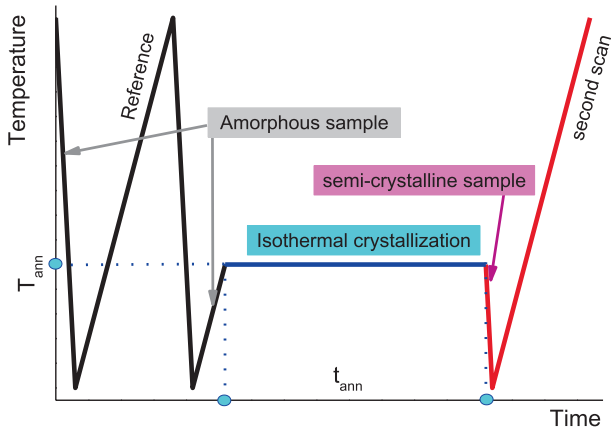

Fig. 2. Temperature profile used in the DSC and BDS experiments.

2.4. Temperature profile – Crystallization experiment parameters

Fig. 2 shows the temperature profile used in the DSC and BDS experiments. In the first scan, we measured the amorphous sample without annealing (reference scan). The second scan measures the semi-crystalline sample after annealing. The isothermal experiments were carried out over a series of crystallization temperatures (T_{ann}) and crystallization times (t_{ann}) to obtain different amounts of ice in each sample. In addition, for the ε-PLL solutions, we used two different cooling rates (fast cooling, 30 K/min, and slow cooling, 5 K/min) to prepare samples with different levels of crystallization. In both cases, the heating rate was 0.5 K/min.

3. Results

3.1. Calorimetric characterization under different crystallization temperatures and times.

Fig. 3 (a-b) shows the total heat flow (HF), the non-reversing heat flow (nRHF), and the reversing heat flow (RHF) of 3PG (c_w = 50-wt%) at a heating rate of 0.5 K/min before (in black) and after (in blue and red) isothermal crystallization. As indicated in the figure, we have used different annealing times (t_{ann}) and temperatures (T_{ann}). For the amorphous sample (reference scan), we can observe the glass transition temperature (overshoot in nRHF) and the cold-crystallization at higher temperatures. After annealing, c_p is lower in the semi-crystalline than in the amorphous state (i.e., Δc_p decreases after crystallization). We can also observe two endothermic peaks in the nRHF. The first one, located at 190 K, is the so-called "overshoot" (which is a manifestation of the recovery of the enthalpy state of the supercooled liquid, and it gives information of the energy released upon aging [36,37]). The second one at higher temperatures (~255 K) is related to the melting peak, and it can be interpreted as the breaking of hydrogen bonds during melting [38].

A significant T_g shift is produced at the highest annealing temperature (T_{ann} = 223 K). However, at T_{ann} = 203 K, T_g does not change before and after crystallization (see Fig. 3b), and only after a long annealing time (t_{ann} = 600 min), it is possible to detect a tiny Δc_p change (see inset of Fig. 4). Therefore, although some nucleation is expected to occur, both the conserved T_g value and the small Δc_p indicate that only a tiny amount of ice is produced in the sample annealed at 203 K.

In addition, Fig. 4 shows temperature scans before and after isothermal crystallization at different heating rates and annealing times. Fig. 4a shows the normalized nRFH, where the crystallization peak strongly depends on the heating rate. Increasing the heating rate of the reference scan, the cold crystallization onset shifts to higher temperatures. The same happens after annealing, although the peak shapes are broader than those in the reference scan and the onset of crystallization temperature ($T_{cryst,on}$) changes to lower temperatures. In the RHF (Fig. 4b), we observe an increase of the signal (exothermic) at temperatures ($T > T_g$), which coincide with the crystallization peaks observed in the non-reversing heat flow part. This observation is discussed in the next section.

Fig. 5 shows the calorimetric response for the ε-PLL solution at two different cooling rates. Crystallization is avoided during the cooling cycle because of the high cooling rate (Fig. 5a). On heating (Fig. 5b), we observe cold crystallization at T = 210 K in the nRHF, whereas the glass transition (at T ~ 195 K) and melting of ice are seen in the RHF. In the second case (not shown), we have annealed a sample using T_{ann} = 205 K with t_{ann} = 192 min. The result indicates that 1 wt% of the water is crystalline, and no T_g shift is observed (T_g ~ 195 K). Finally, in Fig. 5c, there is crystallization on cooling because of the low cooling rate (5 K/min). For this sample, 5.4 wt% of the water is crystalline, and T_g shifts to a slightly higher temperature, T_g = 196 K.

3.2. Dynamical characterization

Now we focus our attention on the dynamics of these solutions in both the amorphous and semi-crystalline states. We have used the same samples to measure the dynamics before and after crystallization. In addition, we have applied the same temperature profile as that used in the calorimetric measurements. The dynamics of amorphous (no annealing) 3PG- and ε-PLL-water solutions were previously analysed [22,23,39–42], and a summary of these results can be seen in Figures S1 to S4 of SI (Supplementary Information). For the 3PG solution [1,39], two dynamic processes (the slower one related to the α-relaxation and the faster due to the reorientation of water molecules) are displayed. In contrast, for the ε-PLL solution, three dynamic processes [23] are observed (the α-relaxation, the slow water relaxation, and the fast water relaxation).

Fig. 6a shows the frequency dependence of the imaginary part of the complex permittivity associated with the α-relaxation and the water relaxation for the amorphous 3PG solution at T = 203 K. Fig. 6b shows the time evolution of the imaginary part of the permittivity (ε″) during isothermal crystallization, using a low annealing temperature (T_{ann} = 203 K) where no T_g change is observed by DSC. At t_{ann} = 0 min (amorphous sample), the water relaxation is located at f ~ $5 \cdot 10^4$ Hz, whereas the α-relaxation can be seen at f ~ $1 \cdot 10^3$ Hz. Increasing the crystallization time, the relaxation times of both water and α-relaxation do not change, although the spectrum becomes broader on the low-frequency side. In addition, a slow extra peak in the spectrum (f ~ 100 Hz) progressively develops while the sample crystallizes, and therefore this dielectric process is related to the presence of ice. Fig. 6c shows the curve fitting for the annealed sample where the contributions from the ice related-, α-, and water relaxations are displayed. Although the relaxation times of the three processes do not change during crystallization (in agreement with the DSC measurements showing that the T_g value does not change because of the low amount of crystallization), the dielectric strength of the water relaxation decreases more than expected from the DSC measurements (see Fig. 6d). However, the relaxation time does not change during the annealing. This implies that concentration and T_g are not changing either. We notice here that the relaxation strength depends on the dipole moment, the density of dipoles, and the correlation between dipoles [43]. The correlation or interaction between water molecules can be induced, for instance, by hydrogen bonding. Therefore, a plausible explanation for the decrease

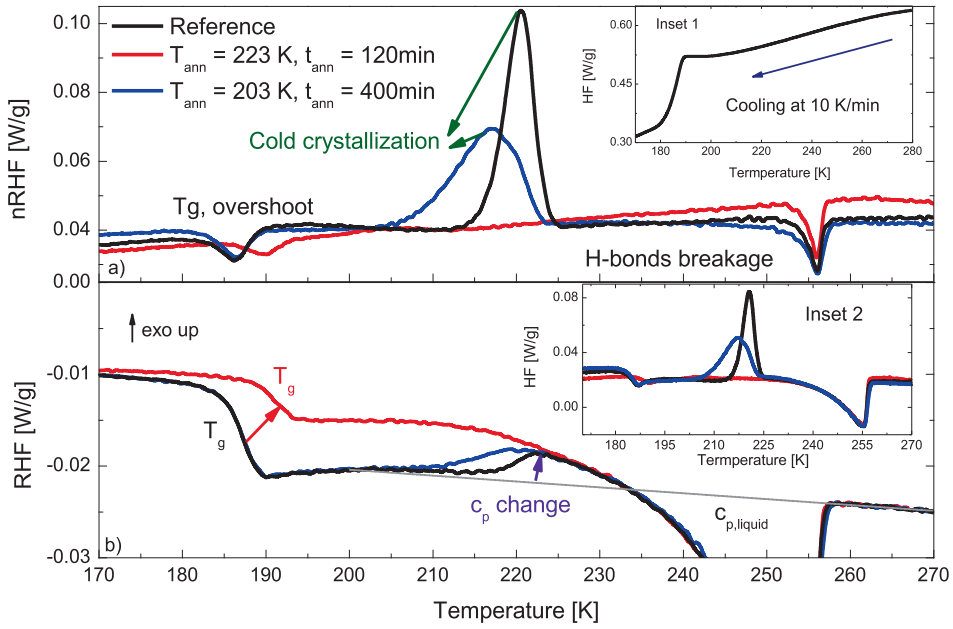

Fig. 3. a) non-Reversing (nRHF) and b) Reversing heat flow (RHF) of 3PG (c_w = 50 wt%) for the amorphous sample (black line) and after annealing at T_{ann} = 223 K and t_{ann} = 120 min (red line) and at T_{ann} = 203 K and t_{ann} = 400 min (blue line). The heating rate was 0.5 K/min. For the reference and the semi-crystalline samples (after T_{ann} = 203 K) a signal jump is produced compared to the $c_{p,liquid}$ baseline (grey line). Inset 1: Cooling scan at 10 K/min. Inset 2: The total heat flow measured on heating is shown. *Inset: Zoom in of the glass transition before (Inset 1) annealing and after the annealing (Inset 2) Colors are the same as in the main plot.*

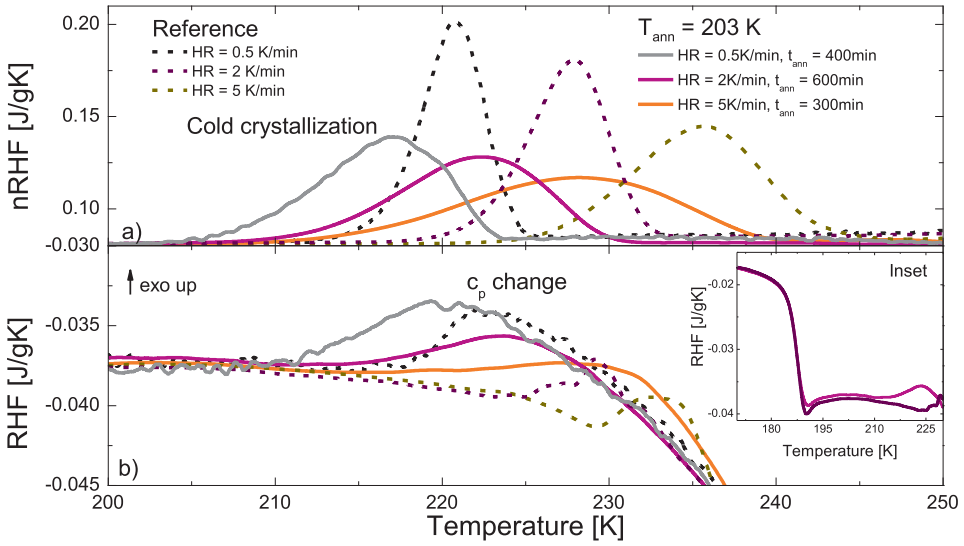

Fig. 4. a) non-reversing heat flow (nRHF) and b) Reversing heat flow (RHF) normalized for different heating rates (0.5, 2 and 5 K/min). The dashed lines represent the reference (amorphous) samples and solid lines represent the second scan (i.e. after isothermal crystallization using T_{ann} = 203 K and t_{ann} = 400, 600 and 300 min respectively). Details of the crystallization peaks and c_p jumps are shown. Inset: Zoom in of the glass transition before and after the annealing. The step size is just slightly smaller after the isothermal crystallization.

of Δε is that the correlation between water molecules changes during annealing, and thus, the relaxation strength decreases, although the relaxation time remains the same. At the same time, the relaxation strength of the ice-related relaxation increases, and that of the α-relaxation slightly decreases with annealing time, implying that water contributes to the α-relaxation of 3PG. A recent article [28] shows an amplitude decrease of the α-relaxation as a consequence of ice formation in ethylene glycol solutions. In this case, ice formation leads to a non-monotonous concentration dependence of the α-process, which does not occur at higher temperatures. The effect is most prominent above T_g because ice formation also reduces the fragility, mitigating the impact near T_g. However, in our case, the dielectric signal is strongly dominated by the ice and water processes significantly above Tg. Therefore, it is not possible to obtain the dynamics of the α-relaxation for the semi-crystalline sample in a broad temperature range to analyse this effect.

Fig. 7 shows the temperature dependences of the relaxation times obtained from fits for the amorphous (a) and semi-crystalline (b) samples at two annealing temperatures (T_{ann} = 203

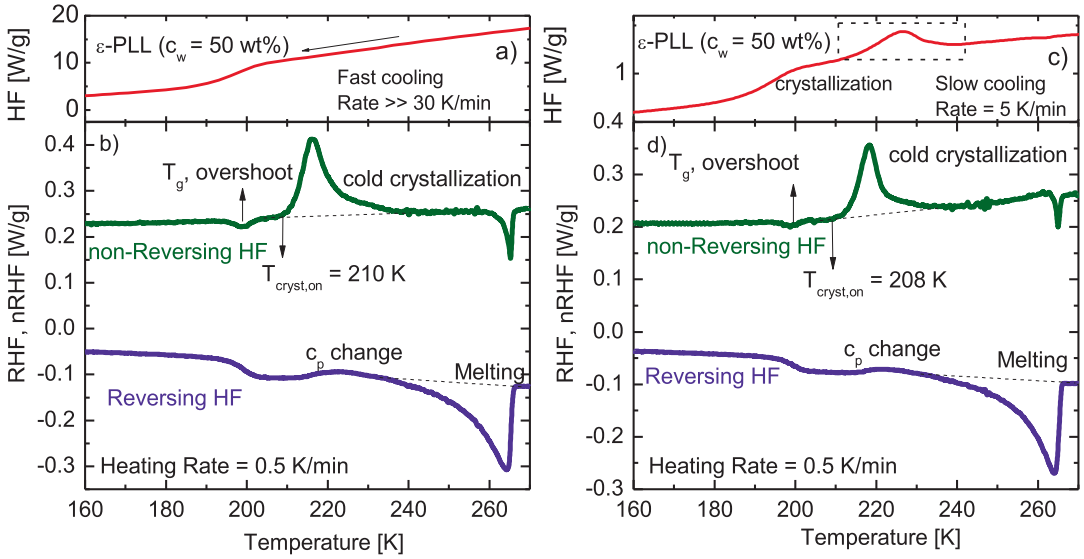

Fig. 5. Calorimetric response of ε-PLL (c_w = 50 wt%) under two different conditions. In (a) the cooling rate exceeds 30 K/min (high) and therefore crystallization on cooling is avoided. In (b) this sample is heated at a rate of 0.5 K/min. In (c) the cooling rate is 5 K/min and therefore there is some crystallization on cooling.

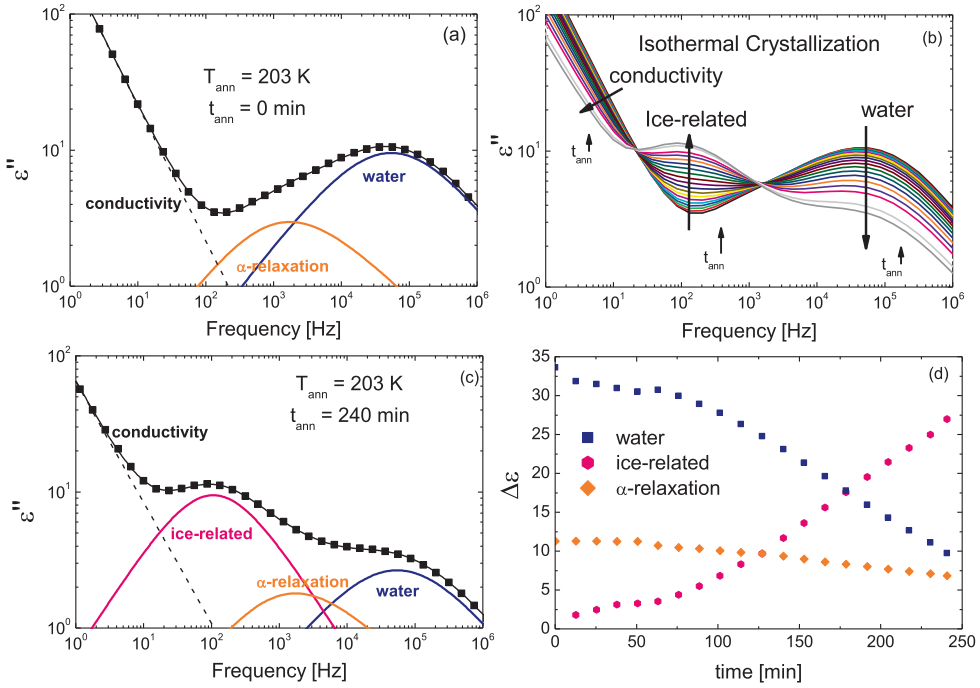

Fig. 6. Loss component, ε", of the complex permittivity, ε*, in the amorphous state (a) and a semi-crystalline state (c). (b) ε" during isothermal crystallization at T_{ann} = 203 K during t_{ann} = 240 min. Curve at t_{ann} = 0 min represents the response of the amorphous material whereas the rest of the curves represent the dynamics after crystallization at different times. (d) Relaxation strengths of the ice-related, water- and α- processes during isothermal crystallization.

and 223 K) for the 3PG solution. For the amorphous sample, we can observe the α- and water relaxations. An apparent single crossover is observed for the water relaxation at T_g (~185 K) for both the amorphous and semi-crystalline (T_{ann} = 203 K) samples. This result can be expected since neither T_g changes for this annealing temperature. However, for the sample annealed at T_{ann} = 223 K, the crossover is produced at a higher temperature (~189 K), also in agreement with the T_g shift found by DSC. The Arrhenius law can describe the water relaxation, $\tau = \tau_0 \cdot \exp(E_a/(k \cdot T))$, regardless of whether the sample is amorphous or semi-crystalline. For the annealing temperature T_{ann} = 203 K the activation energy is E_a = 0.46 eV for the amorphous and semi-crystalline samples, as previously reported [44–46]. In contrast, for the sample annealed at T_{ann} = 223 K, the activation energy is 0.36 eV. This value is in good agreement with that of the ice-affected water reported in [47], which corresponds to interfacial water between the ice and the solute. In the relaxation map of Fig. 7b, we can also observe the ice-related relaxation with an activation energy of 0.39 eV. The ice-related relaxation for the semi-crystalline ε-PLL (c_w = 50-wt%) sample obtained after slow cooling rate has a similar activa-

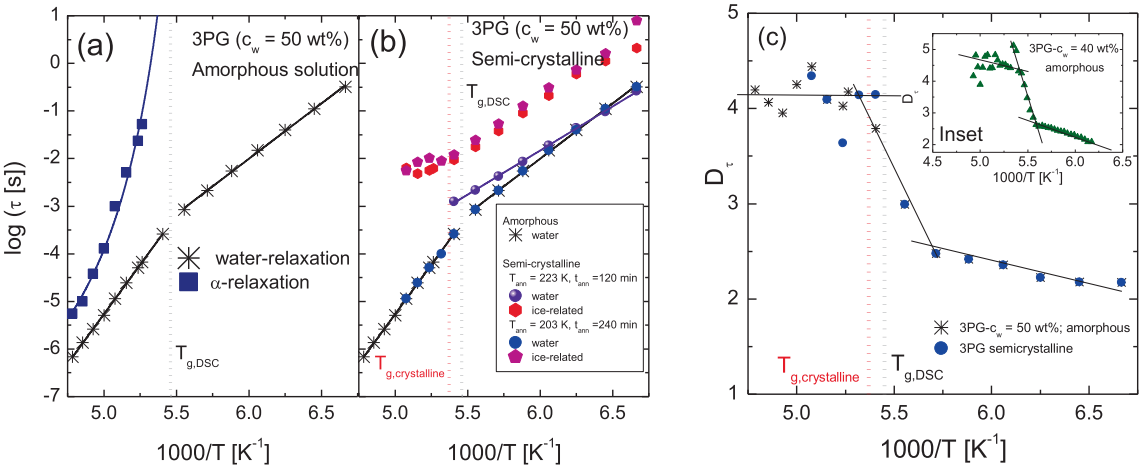

Fig. 7. Temperature dependences of the relaxation times for (a) amorphous and (b) semi-crystalline 3PG-water solutions (c_w = 50 wt%) obtained after annealing at T_{ann} = 203 and 223 K. T_g was obtained by DSC and is shown as dashed lines for all samples. (c) Derivative of the relaxation times (D_τ) of the water relaxation in the amorphous and semi-crystalline states, as shown in Figure (b) Inset: Derivative of relaxation times of 3PG with c_w = 40 wt%.

tion energy as the annealed sample (see Fig. 8 (b) and (c)). However, comparing the semi-crystalline state of 3PG and ε-PLL solutions, the ice-related relaxation times in ε-PLL is almost one order of magnitude slower than that of 3PG (c_w = 50 wt%) and this could be due to the growth of ice in a different environment. Figure S5 shows the temperature dependence of the relaxation times for bulk ice[46,48], ice under confinement [49], and ice in solutions [31,50–53]. It can be seen that the relaxation times for the different ice-related processes differ from each other, and probably each solute affects this relaxation differently. Indeed, the bulk ice relaxation times strongly depend on the preparation protocol [54]. It should also be noted that the ice-related relaxation shows a plateau above T_g (see Fig. 7b), which is also observed in ethylene glycol–water solutions [28]. Water is prone to re-crystalize more quickly above T_g than at lower temperatures and, therefore the water and ice contents are changing very fast, which is the reason for this plateau.

Fig. 7c shows the derivative (D_τ) of the water relaxation times. From the figure, it can be seen that there is a constant value of D_τ above the crossover range (indicating an Arrhenius temperature

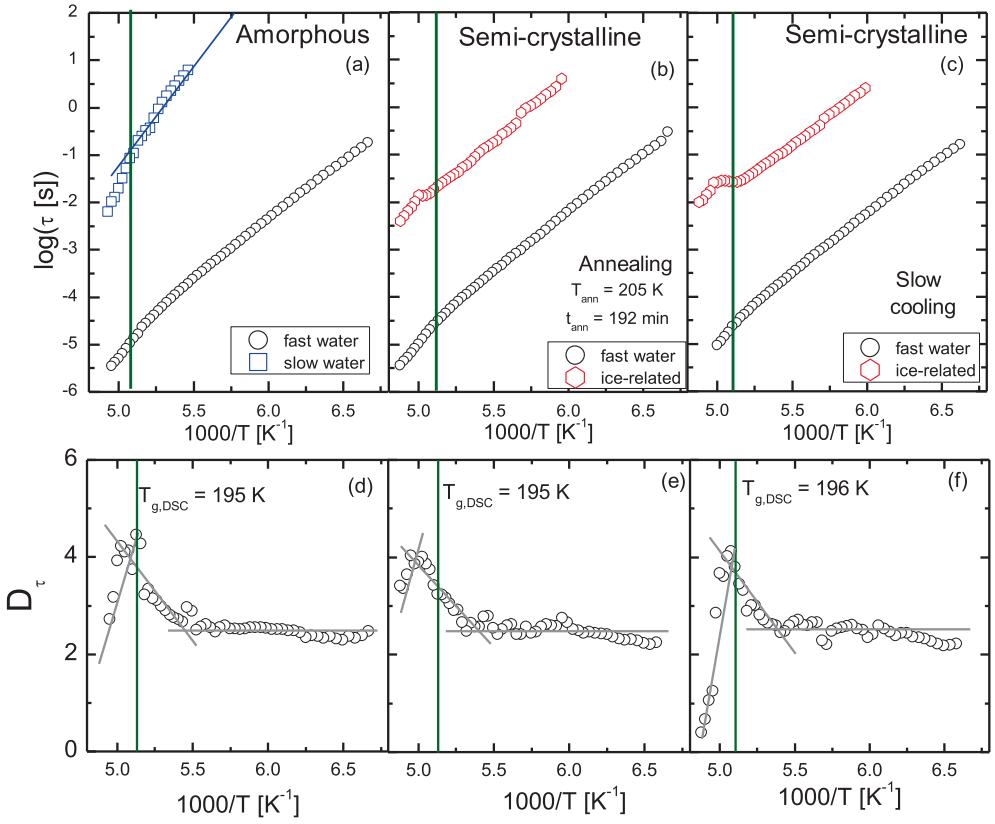

Fig. 8. (a) Temperature dependences of the relaxation times. (a) Amorphous ε-PLL solution, (b) after annealing at T_{ann} = 205 K during 192 min, and (c) for a semi-crystalline sample after slow cooling. (d)-(f) Derivatives of relaxation times of Figures (a)-(c). Vertical green lines (in all the Figures) indicate the onset of the calorimetric T_g.

dependence of the relaxation time). Below the crossover range, a decreasing value of D_τ with decreasing temperature indicates a non-perfect Arrhenius behaviour with a slight decrease of the apparent activation energy. The crossover range starts at about the calorimetric T_g and continues to 10 K below T_g. Thus, partial crystallization does not affect the width (approximately 10 K) of the crossover region.

We now focus on the dynamics of the ε-PLL solution in the temperature range from 150 to 210 K, where cold-crystallization starts. In this restricted temperature interval, only the slow- and fast-water relaxations are observed. Fig. S3 in SI shows the imaginary part of the complex dielectric permittivity from 150 to 200 K, where also the fitting procedure is described (see Figure S4 in SI). Fig. 8 shows the temperature dependence of the fast-water relaxation before and after annealing at different times, as indicated in the plot. We have measured the permittivity every degree to be able to determine the crossover temperature with good accuracy.

Also, in the case of the ε-PLL solutions, it is evident from Fig. 8 (d)-(f) that there is only one crossover and that this is not significantly affected by the partial crystallization. However, in this case, it is obvious that the derivative value D_τ increases rapidly with decreasing temperature above the crossover temperature range. This is typical for a super-Arrhenius temperature dependence, such as VFT. Below the crossover range, the D_τ value is almost constant, as expected for an Arrhenius temperature dependence (the activation energy is about 0.50 eV irrespective of the level of crystallinity). As for the 3PG solutions, the crossover range starts at about T_g and continues to less than 10 K below T_g. Neither for the ε-PLL solution an apparent effect of crystallization on the crossover is observed.

4. Discussion

4.1. Calorimetric results

Crystallization is a process that occurs as a collection of several sub-processes [55]. The first step is the as primary nucleation, where nuclei formation occurs from an initial clear solution. Following this initial nucleation, the growth of crystals occurs [56]. A high-speed cooling scan could avoid crystallization, although nuclei formation is most of the time unavoidable. This is the case shown in Inset 1 of Fig. 3, where the DSC measurement does not detect any crystal formation, but there could be some nuclei. As mentioned, DSC does not detect crystal nuclei. Therefore, even the sample we call ‘‘amorphous” might contain some nucleus generated during cooling.

Table 1 shows the T_g for amorphous and semi-crystalline (T_{ann} = 203 and 223 K) 3PG samples. When the annealing is performed at a low temperature (T_{ann} = 203 K), T_g does not change (since a low amount of ice is produced), whereas, at a high annealing temperature (T_{ann} = 223 K), there is a more considerable T_g change due to a large amount of ice. In addition, the enthalpy of crystallization is almost identical for samples annealed at 203 K during different times (300, 400, and 600 min, Fig. 4), indicating that basically the same amount of ice is produced independent of the heating rate. In fact, after 600 min only (5.75 ± 1.15) % of the water had crystallized. Thus, T_g and Δc_p of the amorphous solutions, are not significantly affected by this small quantity of ice, probably because this low annealing temperature, just above T_g, favored the nuclei formation but not the succeeding growth of the nuclei (this can be also seen in Fig. 6d where $\Delta\varepsilon$ of water decreases). However, after annealing at T_{ann} = 223 K, (26 ± 2) % of water had crystallized, which causes T_g to increase and Δc_p to decrease due to a corresponding reduction of the amount of non-crystalline water. This change of c_p after crystallization not only occurs for water but also for any homo-polymer [57,58]. As shown in Fig. 3b, above T_g and below the cold-crystallization temperature, c_p agrees with the heat capacity of the liquid ($c_{p,liquid}$) for the amorphous and semi-crystalline samples (T_{ann} = 203 K, see Fig. 3b). Simultaneously, with the starting of cold-crystallization (Fig. 3b), a c_p jump is produced, which is seen as an exothermic peak in the RHF (Fig. 3a). Murata and Tanaka [16] observed a similar exothermic peak in the reversing heat flow of water/1,2,4-butanetriol mixtures. In that paper, this feature was interpreted as a liquid–liquid transition of water. However, this exothermic peak is caused by a change of the concentrations in the solution. This was also analyzed by Zhao and coworkers [25] in glycerol-water mixtures and they concluded that the “liquid II phase of water” refers to a freeze-concentrated phase obtained by annealing. Moreover, this behavior was also observed after crystallization of pure poly(3-hydroxybutyrate) [58] or pure ethylene glycol [59]. For both pure materials, an abrupt decrease of c_p in the RHF was observed simultaneously with the cold-crystallization. Thus, we conclude that the heat capacity of water mixtures varies during crystallization, due to an associated change in the phase composition. Therefore, the decrease of c_p is related to the occurrence of cold-crystallization.

Table 2 shows the results for the ε-PLL solutions. In this case, we did not generate a large amount of ice (only 1 and 5.4 wt% of water is crystalline) by the annealing and therefore T_g is not appreciably changing for any of the protocols used.

4.2. Dynamics –fast water relaxation

We have presented results of the dynamics of water in conventional and bio solutions in both the amorphous and semi-crystalline states with different ice contents. When the samples were annealed at temperatures close to T_g, the ice content is low, and the glass transition does not change compared to the amorphous state. In this case, the dynamics also remains the same. We have shown this case in Fig. 7b for 3PG solutions using T_{ann} = 203 K, and in Fig. 8b for ε-PLL solutions using T_{ann} = 205 K. By contrast, when the ice level increases, the unfreeze-concentrated phase changes and, consequently, T_g increases and

Table 1
T_g (onset) for 3PG (c_w = 50 wt%) in the amorphous and semi-crystalline state (after annealed at T_{ann} during t_{ann}). ΔH_{crsyt} is the enthalpy of crystallization calculated as the area of the cold crystallization peak.

Sample	T_{ann} [K]	t_{ann} [min]	Heating rate [K/min]	ΔH_{crsyt} [J/g]	T_g [K]
3PG amorphous state	–	–	0.5	34.7	185.0
			2		
			5		
3PG semi-crystalline state	203	300	5	33 ± 2	185.0
		400	0.5	31 ± 2	
		600	2	31 ± 2	
	223	120	2	–	189.0

Table 2
T_g (onset) for ε-PLL (c_w = 50 wt%) in the amorphous and semi crystalline state (after annealed at T_{ann} during t_{ann}). ΔH_{crsyt} is the enthalpy of crystallization calculated as the area of the cold crystallization peak.

Sample	T_{ann} [K]	t_{ann} [min]	Cooling rate [K/min]	Heating rate [K/min]	ΔH_{crsyt} [J/g]	T_g [K]
ε-PLL - amorphous state	–	–	≫ 30	0.5	34.8	195
ε-PLL semi-crystalline state	205	192	≫30	0.5	33.4	195
	–	–	5	0.5	8.5 / 26.6	196

the dynamics changes accordingly. This is the case shown in Fig. 7b for the 3PG solution after annealing at T_{ann} = 223 K.

In both types of solutions, we detected the same phenomenological behaviour; the fast water relaxation displays a single crossover in the temperature dependence of its relaxation time, irrespective of the degree of crystallization. This is shown in Fig. 9, where the derivate of the relaxation times of ε-PLL (c_w = 50-wt%) and 3PG (c_w = 40 wt%) are displayed (3PG with 50 wt% of water was previously shown in Fig. 7c). In this case, to be more precise in the derivative analysis, we measured the dielectric response each one degree. The calorimetric glass transition temperature, from its onset to its end (see the grey area), is also shown in the same figure. The onset of the crossover is clearly occurring in the middle of the calorimetric T_g-range as reported by us and several other investigations of the dynamics of water in solutions [5,18,20,29]. However, the reason for a lack of a second dynamic crossover due to partial crystallization may be that the BDS measurements were performed from low to high temperatures, i.e., no additional crystallization occurred during the temperature scan. On the other hand, the activation energy of the water relaxation was not substantially affected by the partial crystallization (only a clear difference for the 3PG sample containing the highest amount, (26 ± 2) %, of ice). This indicates that a measurement during heating, with ice formation during cooling (before the measurement), would not cause a clear change of the activation energy of the water, i.e. no evident dynamical crossover.

The question is, why partial ice formation has such a minor influence on the water dynamics and its dynamic crossover? A possible answer to this question is that when ice starts to form, the ice crystals grow and tend to aggregate into larger ice clusters, leading to micro-phase separation of the amorphous and crystalline regions. This implies that the presence of ice will have very little influence on the dynamics in the amorphous regions, except for the effect of freeze concentration. Since the effect of freeze concentration is only significant for the 3PG sample with the highest amount of ice (26 ± 2%), the water relaxation was only altered in this sample.

4.3. Comparison between highly asymmetric mixtures of liquids and water mixtures

Recently, it was suggested in the literature that the dynamics of protein-water [60] or polymer-water [61] mixtures have similar characteristics to those of highly asymmetric mixtures of two glass-formers or polymers. These systems, called HAM (highly asymmetric mixtures), were intensely studied in the literature [62–65]. HAM refers to the mixture of two polymer or glass-formers (A and B) with glass transition temperatures $T_{g,A} \gg T_{g,B}$. If we can find parallelism between protein solutions and HAM, it could be an essential finding to understand the dynamics of protein solutions.

In the case of a mixture with two components (A and B), we know that from high temperatures, we can see the dynamics (α_A relaxation) of component A (high-T_g component), which extrapolated to 100 s coincides with the calorimetric $T_{g,A}$. At lower temperatures, the dynamics of component B (α_B relaxation) change from VFT to Arrhenius behavior at $T_{g,A}$. The relaxation time of component B reaches 100 s at $T_{g,B}$ detected by DSC. The component B, changes to Arrhenius at $T \approx T_{g,A}$ because B is confined by the frozen matrix A. Both α_A and α_B relaxation are mainly controlled by the component A and B respectively and, in both cases there are participation of the other component (B and A respectively). For these mixtures, a secondary relaxation is observed below T_g.

The scenario explained above for HAM could be very similar to what we show in Fig. 1b for biological solutions, considering component A as the solute (ε-PLL) and component B as the solvent (water). Therefore, as previously suggested [60], we wonder whether the dynamic crossovers in water mixtures can be connected with those observed in highly asymmetric polymer blends or mixtures of two liquids.

The first consideration to establish this parallelism is that we can only observe one glass transition temperature by DSC. This coincides with the temperature where the solute relaxation reaches 100 s, and the water relaxation exhibits a dynamic crossover. In the case of biological solutions with two water relaxations at low temperatures, both relaxations undergo a dynamic cross-

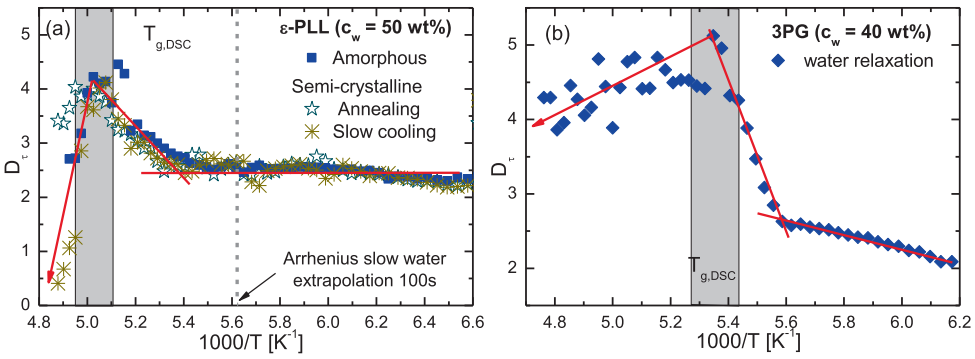

Fig. 9. Derivate of the relaxation times of the fast water relaxation of (a) ε-PLL with c_w = 50 wt% and (b) 3PG with c_w = 40 wt%. In both types of solutions, only a single crossover is seen.

over at T_g of the solute. However, there is no detected calorimetric T_g for the water and neither any additional dynamic crossover. Thus, there is a dynamic crossover at $T_{g,A}$, but no $T_{g,B}$ or additional dynamic crossover in the case of biological solutions. Moreover, this scenario is also observed for 3PG mixtures, where no component A (α-$_A$ relaxation) is seen. This fact is against a direct similarity between HAM and water mixtures.

5. Conclusions

In summary, we have provided calorimetric and dielectric data on conventional and bio-like solutions in both amorphous and semi-crystalline states. We find only a single dynamic crossover in the temperature dependence of the relaxation time for the water relaxation process of conventional solutions and the fast water relaxation process of bio-like solutions. This crossover is produced at the calorimetric T_g, or some degrees below T_g. It is also evident that partial ice formation has only a minor influence on the water dynamics and the calorimetric T_g. A reason for this is likely that the formed ice crystals grow and tend to aggregate into larger ice clusters, leading to micro-phase separation of the amorphous and crystalline regions. This implies that the crystalline regions will not affect the dynamics in the amorphous regions more than the effect freeze concentration gives rise to.

We cannot establish direct parallelism between highly asymmetric mixtures and water mixtures studied here. For example, we cannot detect two glass transitions by DSC, despite two cooperative dynamical processes (α-relaxation and the slow water relaxation) which vitrify at two different temperatures. A possible reason for this might be that the slow-water relaxation also exhibits a dynamic crossover to a low temperature Arrhenius behavior at the single calorimetric T_g. Thus, the cooperativity of the slow-water relaxation seems to disappear at T_g of the other component, and therefore it does not give rise to any additional glass transition.

CRediT authorship contribution statement

Jorge H. Melillo: Formal analysis, Writing – original draft. **Jan Swenson:** Investigation, Funding acquisition. **Silvina Cerveny:** Conceptualization, Investigation, Supervision, Funding acquisition.

Declaration of Competing Interest

The authors declare that they have no known competing financial interests or personal relationships that could have appeared to influence the work reported in this paper.

Acknowledgement

Financial support through the Grant Nos. PID2019-104650 GB-C21 (MICINN-Spain and FEDER-UE), LINKB20012 (CSIC), and IT1566-22 (Basque Government) are gratefully acknowledged, as well as the Grant No. 2019-04020 from the Swedish Research Council. We acknowledge support of the publication fee by the CSIC Open Access Publication Support Initiative through its Unit of Information Resources for Research (URICI).

Appendix A. Supplementary material

Supplementary data to this article can be found online at https://doi.org/10.1016/j.molliq.2022.119039.

References

[1] S. Cerveny, J. Colmenero, A. Alegria, J. Non-Cryst. Solids 353 (2007) 4523.
[2] S. Cerveny, J. Colmenero, A. Alegria, European Phys. J. Special Topics 141 (2007) 49.
[3] H. Frauenfelder, G. Chen, J. Berendzen, P.W. Fenimore, H. Jansson, B.H. McMahon, I.R. Stroe, J. Swenson, R.D. Young, PNAS 106 (2009) 5129.
[4] S. Friesen, M.V. Fedotova, S.E. Kruchinin, R. Buchner, PCCP 23 (2021) 1590.
[5] A. Panagopoulou, A. Kyritsis, R. Sabater i Serra, J.L. Gómez Ribelles, N. Shinyashiki, P. Pissis, Biochimica et Biophysica Acta (BBA) - Proteins and Proteomics 1814 (2011) 1984.
[6] P. Roy, S. Menon, N. Sengupta, J Phys. Chem. B 126 (2022) 44.
[7] O.A. Dmitriev, M.V. Fedotova, R. Buchner, PCCP 19 (2017) 20474.
[8] D. Sauer, B. Schuster, M. Rosenstihl, S. Schneider, V. Talluto, T. Walther, T. Blochowicz, B. Stuhn, M. Vogel, J. Chem. Phys. 140 (2014).
[9] K.E. Zachariassen, E. Kristiansen, Cryobiology 41 (2000) 257.
[10] D. Laage, T. Elsaesser, J.T. Hynes, Chem. Rev. 117 (2017) 10694.
[11] M.C. Bellissent-Funel, A. Hassanali, M. Havenith, R. Henchman, P. Pohl, F. Sterpone, D. van der Spoel, Y. Xu, A.E. Garcia, Chem. Rev. 116 (2016) 7673.
[12] R.J. Speedy, C.A. Angell, J. Chem. Phys. 65 (1976) 851.
[13] H.E. Stanley, J. Teixeira, A. Geiger, R.L. Blumberg, Physica A 106 (1981) 260.
[14] P.H. Poole, F. Sciortino, U. Essmann, H.E. Stanley, Nature 360 (1992) 324.
[15] O. Mishima, H.E. Stanley, Nature 396 (1998) 329.
[16] K.-I. Murata, H. Tanaka, Nat. Commun. 4 (2013) 2844.
[17] P. Gallo, K. Amann-Winkel, C.A. Angell, M.A. Anisimov, F. Caupin, C. Chakravarty, E. Lascaris, T. Loerting, A.Z. Panagiotopoulos, J. Russo, J.A. Sellberg, H.E. Stanley, H. Tanaka, C. Vega, L. Xu, L.G.M. Pettersson, Chem. Rev. 116 (2016) 7463.
[18] J. Swenson, S. Cerveny, J. Phys.: Condens. Matter 27 (2015) 033102.
[19] M. Vogel, Phys. Rev. Lett. 101 (2008) 225701.
[20] S. Cerveny, F. Mallamace, J. Swenson, M. Vogel, L. Xu, Chem. Rev. 116 (2016) 7608.
[21] H. Jansson, F. Kargl, F. Fernandez-Alonso, J. Swenson, J. Chem. Phys. 130 (2009).
[22] I. Combarro Palacios, C. Olsson, C.S. Kamma-Lorger, J. Swenson, S. Cerveny, J. Chem. Phys. 150 (2019) 124902.
[23] S. Cerveny, I. Combarro-Palacios, J. Swenson, J. Phys. Chem. Lett. 7 (2016) 4093.
[24] J. Swenson, PCCP 20 (2018) 30095.
[25] L.-S. Zhao, Z.-X. Cao, Q. Wang, Sci. Rep. 5 (2015) 15714.
[26] S. Cerveny, S. Ouchiar, G.A. Schwartz, A. Alegria, J. Colmenero, J. Non-Cryst. Solids 356 (2010) 3037.
[27] K.-I. Murata, H. Tanaka, Nat. Mater. 11 (2012) 436.
[28] M. Reuhl, P. Monnard, M. Vogel, J. Chem. Phys. 155 (2021) 224501.
[29] C. Gainaru, A. Fillmer, R. Bohmer, J. Phys. Chem. B 113 (2009) 12628.
[30] K. Sasaki, R. Kita, N. Shinyashiki, S. Yagihara, J. Chem. Phys. 140 (2014).
[31] K. Sasaki, A. Panagopoulou, R. Kita, N. Shinyashiki, S. Yagihara, A. Kyritsis, P. Pissis, J. Chem. Phys.B 121 (2017) 265.
[32] I. Popov, A. Puzenko, A. Khamzin, Y. Feldman, PCCP 17 (2015) 1489.
[33] I. Popov, I. Lunev, A. Khamzin, A. Greenbaum, Y. Gusev, Y. Feldman, PCCP 19 (2017) 28610.
[34] D. Agranovich, P. Ben Ishai, G. Katz, D. Bezman, Y. Feldman, Colloids and Surfaces B-Biointerfaces 141 (2016) 390.
[35] Y. Kurzweil-Segev, A. Greenbaum, I. Popov, D. Golodnitsky, Y. Feldman, PCCP 18 (2016) 10992.
[36] O. Delcourt, M. Descamps, J. Even, M. Bertault, J.F. Willart, Chem. Phys. 215 (1997) 51.
[37] I.M. Hodge, A.R. Berens, Macromolecules 15 (1982) 762.
[38] J. Zhao, H. Wang, J. Polym. Sci., Part B: Polym. Phys. 54 (2016) 1869.
[39] S. Cerveny, G.A. Schwartz, A. Alegria, R. Bergman, J. Swenson, J. Chem. Phys. 124 (2006) 194501.
[40] S. Cerveny, J. Swenson, J. Chem. Phys. 150 (2019) 234904.
[41] M. Weigler, I. Combarro-Palacios, S. Cerveny, M. Vogel, J. Chem. Phys. 152 (2020) 234503.
[42] J.H. Melillo, J.P. Gabriel, F. Pabst, T. Blochowicz, S. Cerveny, PCCP 23 (2021) 15020.
[43] F. Kremer, A. Schönhals (Eds.), Broadband Dielectric Spectroscopy, Springer Berlin Heidelberg, Berlin, Heidelberg, 2003.
[44] G.P. Johari, S.J. Jones, J. Chem. Phys. 62 (1975) 4213.
[45] G.P. Johari, S.J. Jones, F.C. Frank, Proceedings of the Royal Society of London, A. Mathematical and Physical Sciences 349 (1976) 467.
[46] G.P. Johari, E. Whalley, J. Chem. Phys. 75 (1981) 1333.
[47] I. Popov, A. Greenbaum, A.P. Sokolov, Y. Feldman, PCCP 17 (2015) 18063.
[48] R.P. Auty, R.H. Cole, J. Chem. Phys. 20 (1952) 1309.
[49] M. Weigler, M. Brodrecht, G. Buntkowsky, M. Vogel, J. Chem. Phys B 123 (2019) 2123.
[50] R.E. Grimm, D.E. Stillman, S.F. Dec, M.A. Bullock, J. Phys. Chem. B 112 (2008) 15382.
[51] T. Yasuda, K. Sasaki, R. Kita, N. Shinyashiki, S. Yagihara, J. Phys. Chem. B 121 (2017) 2896.
[52] Y. Kurzweil-Segev, I. Popov, I. Solomonov, I. Sagit, Y. Feldman, J. Phys. Chem. B 121 (2017) 5340.
[53] N. Shinyashiki, W. Yamamoto, A. Yokoyama, T. Yoshinari, S. Yagihara, R. Kita, K. L. Ngai, S. Capaccioli, J. Phys. Chem. B 113 (2009) 14448.
[54] K. Sasaki, R. Kita, N. Shinyashiki, S. Yagihara, J. Phys. Chem. B 120 (2016) 3950.
[55] J. McGinty, N. Yazdanpanah, C. Price, J.H. ter Horst, J. Sefcik, The Handbook of Continuous Crystallization, Royal Soc. Chem. (2020) 1–50.
[56] R.W. Rousseau, in: Encyclopedia of Physical Science and Technology (Third Edition), Academic Press, New York, 2003, pp. 91–119.
[57] M.L. Di Lorenzo, R. Androsch, A.M. Rhoades, M.C. Righetti, in: Handbook of Thermal Analysis and Calorimetry, Elsevier Science, B.V., 2018, pp. 253–299.

[58] M.L. Di Lorenzo, M. Gazzano, M.C. Righetti, Macromolecules 45 (2012) 5684.
[59] A. Toxqui-Terán, C. Leyva-Porras, M.Á. Ruíz-Cabrera, P. Cruz-Alcantar, M.Z. Saavedra-Leos, Polymers 10 (2018) 467.
[60] S. Capaccioli, L. Zheng, A. Kyritsis, A. Paciaroni, M. Vogel, K.L. Ngai, ACS Omega 6 (2021) 340.
[61] K. Sasaki, M. Takatsuka, N. Shinyashiki, K.L. Ngai, J. Mol. Liq. 333 (2021) 115907.
[62] S. Schramm, T. Blochowicz, E. Gouirand, R. Wipf, B. Stühn, Y. Chushkin, J Chem. Phys. 132 (2010) 224505.
[63] T. Blochowicz, S. Schramm, S. Lusceac, M. Vogel, B. Stühn, P. Gutfreund, B. Frick, Phys. Rev. Lett. 109 (2012) 035702.
[64] T. Körber, R. Minikejew, B. Pötzschner, D. Bock, E.A. Rössler, The European Physical Journal E 42 (2019) 143.
[65] K.L. Ngai, S. Valenti, S. Capaccioli, J. Non-Cryst. Solids 558 (2021) 119573.